Evaluation of the Jacobians of Infrared Radiation Models for Variational Data Assimilation

Frederic Chevallier, Jean-François Mahfouf

Evaluation of the Jacobians of Infrared Radiation Models for Variational Data Assimilation

FRÉDÉRIC CHEVALLIER AND JEAN-FRANÇOIS MAHFOUF

European Centre for Medium-Range Weather Forecasts, Reading, Berkshire, United Kingdom

(Manuscript received 20 May 2000, in final form 15 November 2000)

ABSTRACT

In this paper, linearized versions of fast infrared radiative transfer schemes for variational data assimilation are studied. A neural network–based infrared broadband radiation model (NeuroFlux) is compared with the European Centre for Medium-Range Weather Forecasts operational radiation model. Also, the Radiative Transfer for Television and Infrared Observation Satellite Operational Vertical Sounder (RTTOV) scheme for satellite brightness temperature computation is compared with a more physically based scheme: the narrowband Synsatrad model developed at the European Organization for the Exploitation of Meteorological Satellites. The Jacobians are examined. They are converted into flux perturbations with the tangent-linear approximation and into atmospheric variable increments with a one-dimensional variational assimilation system. For NeuroFlux and RTTOV, despite accurate flux and radiance computation, the sensitivity with respect to water vapor needs to be improved. However, the random structure of the neural network derivative error allows the use of NeuroFlux with a single mean Jacobian in the variational context. Also, further improvements to RTTOV are expected from ongoing work on the regression dataset and on the choice of the regression predictors.

1. Introduction

A variational algorithm adjusts a set of control variables to minimize a function of these variables. Variational algorithms have been increasingly used in data assimilation for numerical weather prediction. They are particularly suitable to derive statistically optimal descriptions of the atmospheric state (the so-called analyses of the operational weather centers) used to provide initial conditions for forecast models. In this case, the function, called a cost function, essentially consists of two terms: the first one quantifies the fit of the model state to available observations and the second one quantifies its fit to a prior estimate (usually a short-range forecast from a previous analysis), given statistics of observation and background errors. The principle of variational data assimilation has been known for several decades (e.g., Sasaki 1958; Lewis and Derber 1985; Le Dimet and Talagrand 1986). However, its high computational cost has made it operationally available only recently. At the European Centre for Medium-Range Weather Forecasts (ECMWF), a three-dimensional variational assimilation system (Courtier et al. 1998) replaced a previous scheme based on optimal interpolation (Hollingsworth 1987) in 1996. The inclusion of the time dimension of observations in the analyses was achieved in 1997 with a four-dimensional variational assimilation system (4D-Var) as described by Courtier et al. (1994). An important consequence of the recent introduction of variational data assimilation in the operational weather centers is the necessity of accurate parameterizations in the analysis procedure not only in terms of atmospheric fluxes but also in terms of partial derivatives of the fluxes with respect to atmospheric variables (i.e., the Jacobians). These derivatives are needed to estimate the gradient of the cost function during the minimization. This is placing an extra demand on modelers, because it increases the requirements for the validation of physical parameterization schemes. Moreover, a minimization process is time consuming when the description of the control variables is global. Therefore, only fast physical parameterizations can be linearized for global variational analyses of the atmosphere. Examples of physical parameterizations for 4D-Var can be found in Janisková et al. (1999) and in Mahfouf (1999).

This study examines two infrared radiation schemes for application in 4D-Var. They use different parameterizations because developments have been performed independently. The first model is a fast scheme for radiative flux computation that has been developed by Chéruy et al. (1996) and Chevallier et al. (1998). This scheme is based on artificial neural networks. The second one is the Radiative Transfer for Television and Infrared Observation Satellite (TIROS) Operational Vertical Sounder (RTTOV; Eyre 1991; Saunders et al.

Corresponding author address: F. Chevallier, ECMWF, Shinfield Park, Reading, Berkshire RG29AX, United Kingdom.
E-mail: f.chevallier@ecmwf.int

1999) for satellite radiance computation. Each scheme is validated here for variational assimilation by comprehensive comparison with a more physically based scheme: respectively, the ECMWF operational wideband model developed by Morcrette (1991) and the narrowband ''Synsatrad'' model (Tjemkes and Schmetz 1997). Estimating the quality of their Jacobians is not trivial. For a better understanding of the differences, they are converted into flux perturbations with the tangent-linear approximation and into atmospheric variable increments with a one-dimensional variational assimilation system (1D-Var), in which radiation is the only physical process represented.

The plan of the paper is as follows. A description of the four infrared radiation models is given in section 2. Section 3 presents the general formalism of 4D-Var and 1D-Var. Section 4 shows the validation of the neural network–based scheme with the ECMWF operational wideband model in a variational framework. The comparison between RTTOV-5 and Synsatrad is detailed in section 5. Section 6 provides an overall summary.

2. Description of the radiation schemes

a. Two schemes for infrared broadband flux computation

The ECMWF operational infrared broadband radiation model (hereinafter EC-OPE) computes the atmospheric fluxes and cooling rates. The cooling rates are the vertical derivatives of the net fluxes at each pressure level. As described by Morcrette (1991), the longwave spectrum from 0 to 2820 cm^{-1} is divided in EC-OPE into six spectral regions. The integration over wavenumber is performed using a band emissivity method. The transmission functions for water vapor and carbon dioxide over the six spectral intervals of the scheme are fitted using Padé approximants on narrowband transmissions obtained with statistical band models. Clouds are represented by multilayer graybodies (Washington and Williamson 1977). Recent improvements to the scheme affect the description of the water vapor continuum and of the ice cloud optical properties, as stated by Gregory et al. (1998). In the ECMWF operational forecast model, radiative fluxes are currently updated once every 3 h and at only sample points to save time in the expensive radiation computations (Morcrette 2000). However, the code is still too slow for use in the variational analysis. Therefore, a very simple longwave radiation model is used in 4D-Var. As described in Mahfouf (1999), it allows perturbations of fluxes and cooling rates to be computed with respect to temperature variations only.

To increase the time–space sampling, a faster version of EC-OPE, called NeuroFlux, has been derived using a statistical approach, the multilayer perceptron defined by Rumelhart et al. (1986), together with the same cloud representation as in EC-OPE: the multilayer graybody model. Consistent with the latter, upward and downward fluxes are computed in NeuroFlux as

$$F(P_i) = \sum_k a_k F_k(P_i), \tag{1}$$

where P_i is the pressure level, F_k is the flux in the presence of a single-layered black cloud in layer k or the clear-sky flux (with the convention $k = 0$ for clear sky), and a_k is a weight. The a_ks are functions of the layered cloud characteristics (cloud cover, liquid and ice water contents, particle size, etc.), (e.g., Ebert and Curry 1992) and depend on the way cloudy layers overlap (e.g., Geleyn and Hollingsworth 1979). In EC-OPE, the F_ks are computed by the method summarized at the beginning of this section, whereas artificial neural networks are used in NeuroFlux. The parameters of the neural networks are derived from EC-OPE using a nonlinear regression. The set of atmospheric profiles used to define the neural network (the learning dataset) is described by Chevallier et al. (2000a). The validation of NeuroFlux showed that it is 7 times faster than the original code, and its accuracy is comparable to the accuracy of the ECMWF operational scheme, with a negligible impact on numerical simulations (Chevallier et al. 2000b).

b. Two schemes for satellite radiance computation

The RTTOV scheme is used operationally at ECMWF for the simulation of satellite brightness temperatures. It can handle instruments like Advanced TIROS Operational Vertical Sounder (ATOVS), Special Sensor Microwave Imager, or Meteosat. Version 5 of this code (Saunders et al. 1999) is used here. The method, originally derived from the work of McMillin et al. (1979), is single band. It is based on two main approximations. The first one is that the Planck function does not vary significantly on the spectral interval considered (the spectral band of the satellite channel), so that a mean value of the Planck function can be introduced for each temperature. The second approximation is the use of a regression fitting to reference convolved line-by-line layer optical depths from the temperature and absorbing gas profiles. The reference line-by-line computations for RTTOV-5 come from the general line-by-line transmittance and radiance model GENLN2, version 4 (Edwards 1992), with a water vapor continuum from the Clough et al. (1989) model, version 2.1. The temperature and absorbing gas profiles used as inputs to the code are described on a fixed 43-level pressure grid.

RTTOV is compared here with Synsatrad, the narrowband scheme developed at the European Organisation for the Exploitation of Meteorological Satellites (EUMETSAT). This method, after Sneden et al. (1975), solves the monochromatic radiative transfer equation at uniformly sampled wavenumbers (Tjemkes and Schmetz 1997). The water vapor continuum refers to the Clough et al. (1989) model, version 2.2. The spectral

resolution of the scheme depends on the channel. As an example, 750 wavenumbers are used for the 6.3-μm channel on the *Meteosat-7* platform, and 500 wavenumbers are used for the 6.3-μm channel on the High-Resolution Infrared Radiation Sounder (HIRS), second generation, on board the NOAA-14 spacecraft. This corresponds to resolutions of 0.67 and 0.28 cm^{-1}, respectively.

The present study focuses on five channels that are of particular interest for operational weather forecasting: the water vapor sounding channels of HIRS aboard *NOAA-14* at 12.5 (HIRS-10), 7.3 (HIRS-11), and 6.3 μm (HIRS-12); the water vapor sounding channel of *Meteosat-7* at 6.3 μm (Meteosat-WV); and the ozone sounding channel of HIRS aboard *NOAA-14* at 9.7 μm (HIRS-09). Restriction is made here to clear-sky modeling. Carbon dioxide and minor absorbing gas concentrations are set to the estimated mean level for 2005. The surface emissivity is set to 1.

3. Generalities about variational assimilation

a. General formalism of 4D-Var

The 4D-Var system seeks an optimal balance between observations and the dynamics of the atmosphere by finding a model trajectory $\mathbf{x}(t)$, which is as close as possible to the observations available during a given time period $[t_0, t_n]$. The model trajectory $\mathbf{x}(t)$ is completely defined by the initial state $\mathbf{x}_0$ at time t_0.

The misfit to given observations $\mathbf{y}^o$ and to an a priori model state $\mathbf{x}^b$ called background is measured by an objective cost function defined as follows:

$$J(\mathbf{x}_0) = \frac{1}{2}(\mathbf{x}_0 - \mathbf{x}_0^b)^{\mathrm{T}}\mathbf{B}^{-1}(\mathbf{x}_0 - \mathbf{x}_0^b) + \frac{1}{2}\sum_{i=0}^{n}\{H_i[\mathbf{x}(t_i)] - \mathbf{y}_i\}^{\mathrm{T}}\mathbf{R}_i^{-1}\{H_i[\mathbf{x}(t_i)] - \mathbf{y}_i\}, \quad (2)$$

where, at any time t_i, $\mathbf{y}_i$ is the vector of observations, H_i is the operator providing the equivalent of the data from the model variable $\mathbf{x}(t_i)$, $\mathbf{R}_i$ is the observation error covariance matrix (measurement errors and representativeness errors, including H_i errors), and $\mathbf{B}$ is the background error covariance matrix of the state $\mathbf{x}^b$. The background $\mathbf{x}^b$ is usually provided by a short-range forecast. Superscripts -1 and T denote an inverse and a transpose matrix, respectively. The subscript i denotes the time index.

In Eq. (2), the observation operator H_i includes a radiative transfer model for the computation of model-equivalent satellite brightness temperatures, similar to RTTOV, if such quantities are assimilated.

The model state $\mathbf{x}(t_i)$ is defined as

$$\mathbf{x}(t_i) = M(t_i, t_0)(\mathbf{x}_0), \quad (3)$$

where M is the nonlinear forecast model integrated from time t_0 to time t_i. The term M may include an infrared radiative transfer model for the computation of fluxes and cooling rates, such as the one described in Mahfouf (1999).

The control vector $\mathbf{x}_0$ includes the prognostic variables to be initialized in the forecast model: vorticity, divergence, temperature, specific humidity, and surface pressure. The minimization uses a descent algorithm, which requires several computations of the gradient of J with respect to the initial state $\mathbf{x}_0$. Given the dimension of the state vector, the adjoint technique is used to provide an efficient estimate of ∇J (Le Dimet and Talagrand 1986):

$$\nabla J(\mathbf{x}_0) = \mathbf{B}^{-1}(\mathbf{x}_0 - \mathbf{x}_0^b) + \sum_{i=0}^{n}\mathbf{M}_i^{\mathrm{T}}\mathbf{H}_i^{\mathrm{T}}\mathbf{R}_i^{-1}\{H_i[\mathbf{x}(t_i)] - \mathbf{y}_i\}, \quad (4)$$

where $\mathbf{H}_i^{\mathrm{T}}$ is the adjoint of the observation operator and $\mathbf{M}_i^{\mathrm{T}}$ is the adjoint of the forecast model.

b. General formalism of 1D-Var

The principle of the 1D-Var is similar to that of 4D-Var, but the control vector $\mathbf{x}$ represents only a single column, and the time dimension is not included. The cost function reduces to

$$J(\mathbf{x}) = \frac{1}{2}(\mathbf{x} - \mathbf{x}^b)^{\mathrm{T}}\mathbf{B}^{-1}(\mathbf{x} - \mathbf{x}^b) + \frac{1}{2}[H(\mathbf{x}) - \mathbf{y}]^{\mathrm{T}}\mathbf{R}^{-1}[H(\mathbf{x}) - \mathbf{y}]. \quad (5)$$

In the following, H is a radiation model, for instance, RTTOV or EC-OPE. The control vector $\mathbf{x}$ contains vertical profiles of temperature, specific humidity, and ozone. Given the low dimension of the control vector, a perturbation method is used to compute the Jacobian elements of the adjoint operator $\mathbf{H}^{\mathrm{T}}$ [i.e., the Jacobian matrix $(\partial y_k/\partial x_l)_{k,l}$]. The term $\mathbf{H}^{\mathrm{T}}$ is required to compute the gradient of the cost function:

$$\nabla J(\mathbf{x}) = \mathbf{B}^{-1}(\mathbf{x} - \mathbf{x}^b) + \mathbf{H}^{\mathrm{T}}\mathbf{R}^{-1}[H(\mathbf{x}) - \mathbf{y}]. \quad (6)$$

The minimizer of the 1D-Var code is a limited-memory quasi-Newton method, the ''M1QN3'' software developed at Institut National de Recherche en Informatique et en Automatique (INRIA) (Gilbert and Lemaréchal 1989). Examples of applications of the 1D-Var code can be found in Marécal and Mahfouf (1999) and Fillion and Mahfouf (2000).

c. The background error covariance matrix

As shown in Eqs. (2) and (5), the error covariance matrix $\mathbf{B}$ plays an essential role in 1D-Var and 4D-Var by determining the spatial distribution of the information on the model variables (McNally 2000). The matrices that are used in the ECMWF 4D-Var are described

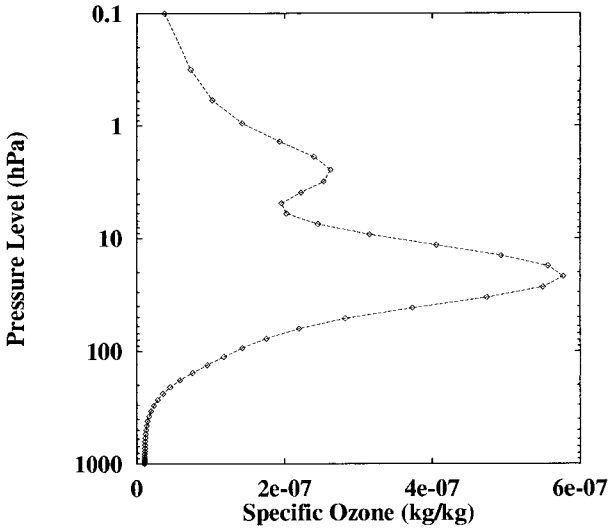

FIG. 1. Profile of background error std dev for unbalanced ozone.

by Rabier et al. (1998) and by Derber and Bouttier (1999). The correlations are estimated by assuming that the difference between forecasts at different ranges valid at the same time is representative of short-range forecast error statistics, as is done by Parrish and Derber (1992). Specific humidity and ozone correlations are sharp on the vertical, whereas atmospheric temperature correlations are broad in the troposphere and in the lower stratosphere, with negative correlations between the two regions. No cross correlation between the background error of temperature, specific humidity, and ozone is used. Mass and wind are coupled through a linear balance operator. The standard deviations of forecast errors for temperature and ozone have been derived with the same approach, whereas the water vapor standard deviations are computed from an empirical formula (Rabier et al. 1998). An example of standard deviations of temperature and humidity is given in Fig. 2 of Fillion and Mahfouf (2000). For temperature, they are about 1 K in the troposphere, with higher values in the stratosphere, up to 4.5 K. The ozone standard deviations for unbalanced quantities (i.e., the fraction of the ozone errors not coupled with wind errors) are shown in Fig. 1.

In the following, **B** is specified according to the operational 4D-Var for unbalanced quantities at the corresponding vertical resolutions. Two vertical resolutions are used here: the 31- and 50-level grids that have been used operationally at ECMWF between 1991 and 1998 and in 1999, respectively. For ozone, standard deviations are taken from the more recent 60-level model, and vertical correlations are set to zero.

4. Validation of NeuroFlux for variational assimilation

a. The multilayer graybody approach in NeuroFlux

As explained in section 2a, NeuroFlux has been derived from a nonlinear regression to the ECMWF operational wideband model (EC-OPE). In the ideal case, its computations would be identical to those of EC-OPE. In fact, the neural network parameterization introduces some uncertainty in the fluxes, cooling rates, and Jacobians. As shown by Chevallier et al. (2000b), the accuracy of the method in terms of fluxes and cooling rates is high enough in the context of a numerical model of the atmosphere. For assimilation purposes, it is also important to have accurate Jacobians.

The Jacobians of NeuroFlux with respect to cloud characteristics are very similar to those of EC-OPE, because both schemes rely on the multilayer graybody approach to treat cloudiness. Indeed, by differentiating Eq. (1), it can be written

$$dF(P_i) = \sum_k a_k dF_k(P_i) + F_k(P_i) da_k. \qquad (7)$$

The da_ks can be computed from the multilayer graybody algorithm, with the same accuracy in NeuroFlux and in EC-OPE. This requires little computing time in comparison with the F_k and dF_k computation. As a consequence, the uncertainty of the dFs computed by NeuroFlux lies in the F_ks and dF_ks. In NeuroFlux, they are computed by neural networks, with comparable accuracy for each value of k.

b. Validation of the Jacobians

As an example of F_k, the clear-sky surface downward longwave flux (SDLF) is considered here. The comparison between the Jacobians of the clear-sky SDLF for temperature and water vapor (i.e., the partial derivative of the flux with respect to temperature or water vapor) computed by NeuroFlux and EC-OPE is shown in Figs. 2a and 2b in the case of a tropical standard atmosphere (McClatchey et al. 1971). All the Jacobian elements for EC-OPE are positive, which means that an increase in water vapor or temperature will increase the SDLF. Sensitivity of the SDLF to temperature is significant only near the surface and then decreases exponentially with height. Its sensitivity to specific humidity is important over a deeper layer of the lower troposphere, up to 600 hPa. The decrease of the Jacobian near the surface comes from the dominance of water vapor absorption.

In comparison with EC-OPE, the Jacobian of NeuroFlux for temperature is irregular, though it is still close to the reference computation. The wiggles originate from the statistical approach of NeuroFlux. Indeed, in a formal neural network, the information is propagated from its inputs to its outputs by nonlinear projections on successive spaces that transform and filter it. The localization of the information, as on a pressure level grid, is partially lost. This has been already observed by Aires et al. (1999) for the modeling of HIRS brightness temperatures. The shape of the Jacobian for water vapor brings more concern. Not only the magnitude of the Jacobian below 600 hPa is underestimated

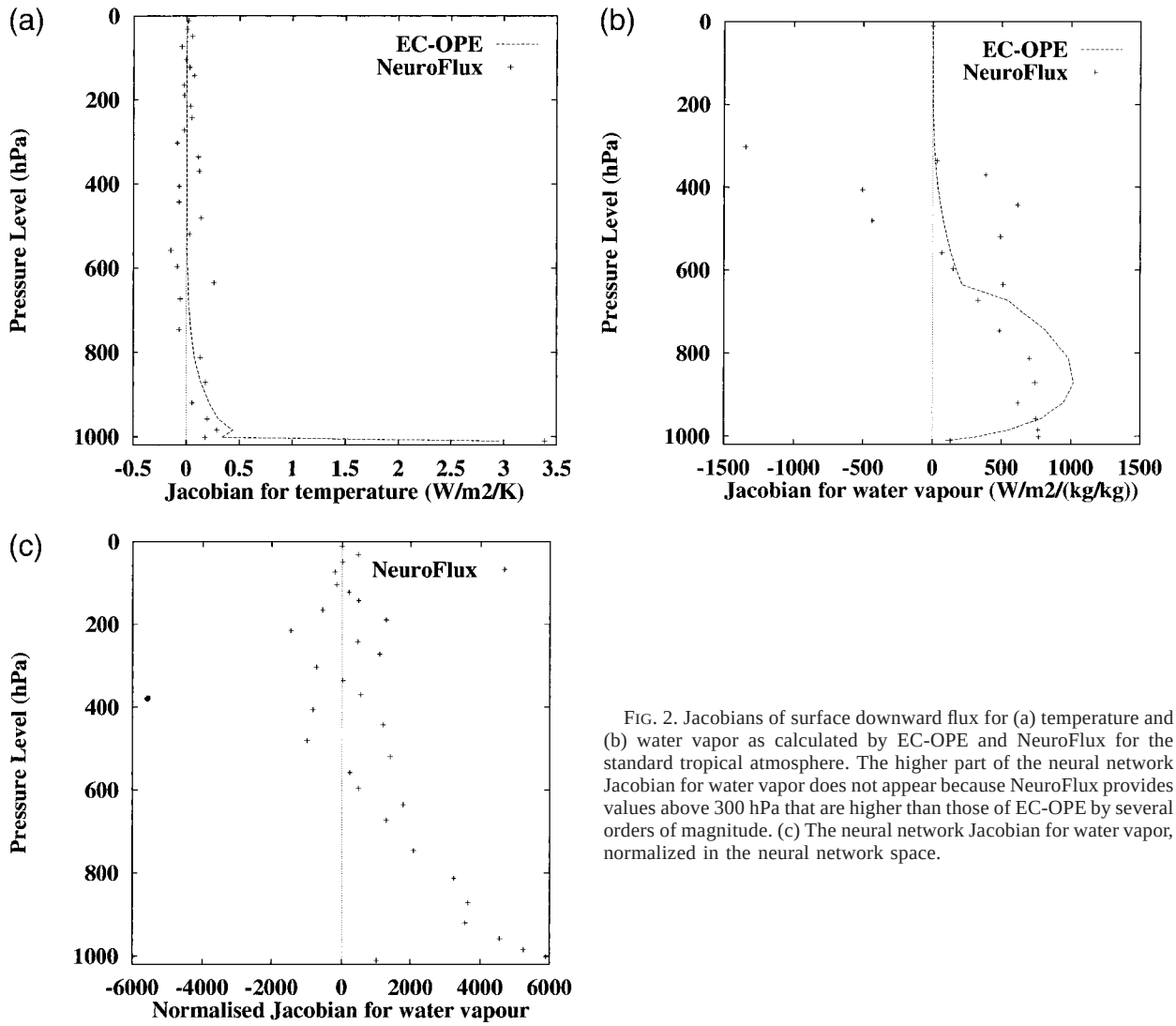

FIG. 2. Jacobians of surface downward flux for (a) temperature and (b) water vapor as calculated by EC-OPE and NeuroFlux for the standard tropical atmosphere. The higher part of the neural network Jacobian for water vapor does not appear because NeuroFlux provides values above 300 hPa that are higher than those of EC-OPE by several orders of magnitude. (c) The neural network Jacobian for water vapor, normalized in the neural network space.

but also NeuroFlux provides derivative values above 600 hPa that are higher than those of EC-OPE by several orders of magnitude. The reason for such irregularities is that, as explained by Chevallier (1998), the input variables to the neural networks are normalized by dividing each variable by its spread in the learning dataset. The normalized Jacobians, as illustrated in Fig. 2c, have limited oscillations. When projected on the physical space using specific humidity as the water vapor variable, they convert into a chaotic profile in the upper atmosphere, where the values of specific humidity are very low.

c. Use of a single mean Jacobian in conjunction with NeuroFlux

The Jacobian weakness of NeuroFlux make it difficult to use them in variational data assimilation if significant water vapor increments are allowed by the **B** matrix [Eq. (2)] above 600 hPa. However, the accurate computation of finite-size perturbations of fluxes by NeuroFlux (Chevallier et al. 2000b) suggests that NeuroFlux could be used to update the fluxes at each iteration of the minimization if a suitable Jacobian is provided by another way for the gradient computation. Such a configuration may solve the problem of computing time posed by EC-OPE.

A single mean Jacobian matrix is built as follows. The global archive of the ECMWF 6-h forecast from 1 March 1998 at 0000 UTC is used to compute a mean temperature and water vapor profile on the 31-level vertical pressure grid. The single mean Jacobian matrix is the Jacobian of this mean profile.

The association of NeuroFlux with the single mean Jacobian matrix is tested for variational assimilation. Two experiments are performed. First, perturbations of cooling rates are computed. Then, a 1D-Var scheme for the assimilation of surface fluxes is evaluated.

1) IMPACT ON THE COMPUTATION OF COOLING RATE PERTURBATIONS

Perturbations of atmospheric temperature, specific humidity, liquid and ice water, cloud cover, and surface temperature are estimated from the difference between the 6-h and the 12-h ECMWF forecasts valid for 1 July 1998 at 0000 UTC. The resolution is 2.5° × 2.5° (10 300 grid points). For instance, the typical size of temperature perturbations is about 1°. Perturbations of longwave cooling rates $\delta_1\mathbf{C}$ are then computed from the model variable perturbations $\delta\mathbf{x}$: $\delta_1\mathbf{C}(\delta\mathbf{x}) = \mathbf{C}(\mathbf{x} + \delta\mathbf{x}) - \mathbf{C}(\mathbf{x})$. Figure 3 presents the mean and standard deviation of the nonlinear cooling rate perturbations computed with EC-OPE with and without cloud–radiation interaction. Three latitude classes are considered: tropical, midlatitude and polar. Without cloud perturbations, standard deviations are below 0.5 K day^{-1}, except near the surface, where they reach 1.5 K day^{-1} on average. Mean values are large only near the surface, where they reach 0.3 K day^{-1} on average for tropical and midlatitude regions. With cloud perturbations, standard deviations increase up to 3.5 K day^{-1}, with some perturbations reaching up to 40 K day^{-1} (not shown).

This dataset is used to validate the single mean Jacobian approach. For the single mean Jacobian approach, as for NeuroFlux, only the accuracy of clear-sky Jacobians matters if the multilayer graybody algorithm is used to parameterize cloud effects. Indeed, from Eq. (7), it appears that

$$\delta F(P_i) \simeq \sum_k a_k \delta F_k(P_i) + F_k(P_i)\delta a_k. \qquad (8)$$

Equation (8) is a good approximation when the perturbations δF_k and δa_k are small ($|\delta F_k| \ll F_k$ and $|\delta a_k| \ll a_k$). For analysis increments, this approximation is valid for δF_k but not for δa_k. Indeed, δa_k can reach the size of a_k. In this case, however, $F_k(P_i)\delta a_k$ is the dominant term in Eq. (8), as seen by the comparison between Figs. 3c and 3d, which makes the approximation still accurate.

To estimate qualitatively the variations of the clear-sky Jacobians, cooling rate perturbations $\delta_2\mathbf{C}$ are computed from the temperature, specific humidity, and surface temperature perturbations of the dataset using a first-order Taylor development: $\delta_2\mathbf{C}(\delta\mathbf{x}) = \mathbf{J}\delta\mathbf{x}$, where $\mathbf{J}$ is the single mean Jacobian matrix defined above. Figure 4 compares the clear-sky nonlinear cooling rate perturbations from EC-OPE $\delta_1\mathbf{C}$ and the linear perturbations $\delta_2\mathbf{C}$. The differences between the two computations originate both from the tangent-linear hypothesis and from the use of a single mean Jacobian matrix. They are comparable to the signal (i.e., the nonlinear perturbations shown in Fig. 3) except below 900 hPa in the tropical and midlatitudes, where the standard deviation of the differences and the bias are significantly smaller than the signal. Improvement in the polar class could be obtained with a standard polar Jacobian. Because the comparison takes the tangent-linear hypothesis into account, the performance of the single mean Jacobian is underestimated. As illustrated below [section 4c(2)], the existence of a clear-sky Jacobian is important from the top of the atmosphere to the surface.

Table 1 completes this study with the statistics of the corresponding boundary fluxes: the outgoing longwave radiation and the surface net fluxes. The error of the tangent-linear computation is significantly below the signal. Indeed, the error standard deviation is less than 60% of the standard deviation of the clear-sky nonlinear computation in every latitude class, with negligible biases (less than 0.2 W m^{-2}).

The variability of the clear-sky Jacobians probably does not play an essential role when computing all-sky flux and cooling rate perturbations. As stated in the beginning of this section, the error of NeuroFlux as compared with EC-OPE only concerns clear-sky modeling. This may allow the use of a single mean Jacobian with NeuroFlux for variational data assimilation. This possibility is investigated further in the next section.

2) IMPACT ON VARIATIONAL ASSIMILATION

The single mean Jacobian approach is tested further in a 1D-Var data assimilation, in which only its contribution determines the increments. Use is made of observations that were collected at Billings, Oklahoma, as part of the Atmospheric Radiation Measurement (ARM) Program (Stokes and Schwartz 1994). A series of five clear-sky days in December of 1997 is selected to evaluate a 1D-Var assimilation of SDLF. Observations of SDLF (from a pyrgeometer) were available on a 2-min basis and were processed to get hourly averages. Corresponding hourly atmospheric profiles for temperature and specific humidity are taken from ECMWF operational short-range forecasts. The profiles and the background statistics [the matrix $\mathbf{B}$ of Eqs. (2) and (5)] are described on a 31-layer vertical grid. The standard deviation of error for the SDLF is set to 10 W m^{-2}, as suggested by the standard for measurements set by the Baseline Surface Radiation Network (Heimo et al. 1993).

The time series of model SDLF and of SDLF from ARM observations are shown in Fig. 5c for the selected five days. The model systematically underestimates the observation fluxes up to 20 W m^{-2}. The reader is referred to Chevallier and Morcrette (2000) for a discussion about these differences. In this context, the 1D-Var iteratively modifies the temperature and water vapor profiles to match better the observed SDLF within a range of background errors given by the covariance matrix $\mathbf{B}$.

The result of the 1D-Var assimilation using the EC-OPE radiation scheme produces a series of longwave fluxes in better agreement with the observations, as expected (Fig. 5c). In agreement with the vertical structure of the Jacobians (Fig. 2), the increase in longwave flux has been done mostly through an increase of water vapor

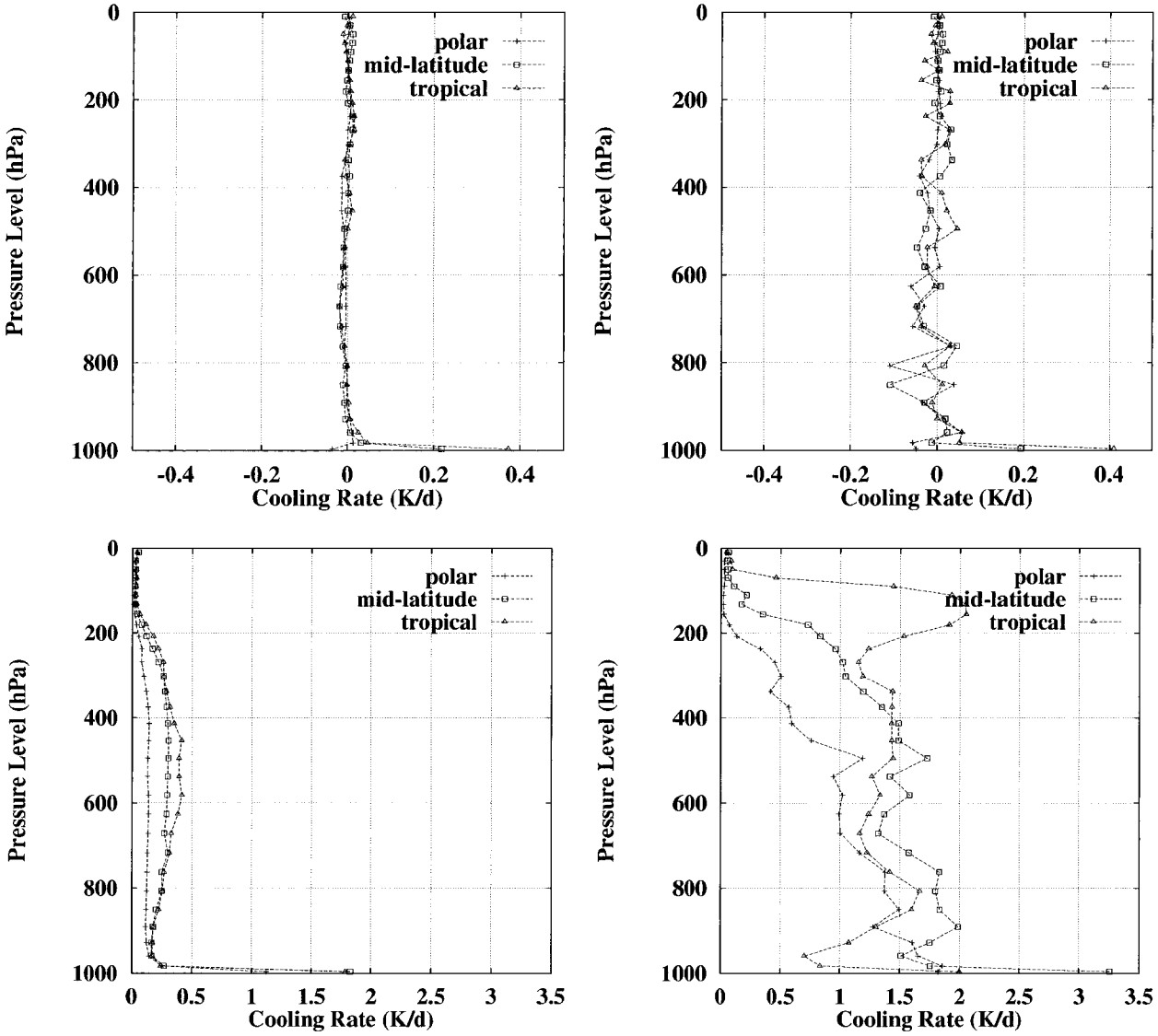

FIG. 3. (top) Mean and (bottom) std dev of the (left) clear-sky and (right) total-sky nonlinear cooling rate perturbations (K day^{-1}). The perturbations are taken from the difference between the ECMWF 6- and 12-h forecasts for 0000 UTC 1 Jul 1998. Results are shown in three latitude classes.

in the atmospheric column. The time series of the total column water vapor is shown in Fig. 5d.

In the single mean Jacobian approach, NeuroFlux is used in the 1D-Var to update the SDLF at each iteration of the minimization, whereas the single mean Jacobian matrix is used to compute the gradient of the cost function. Figures 5a and 5b show that the increments of SDLF and of total column water vapor computed by the single mean Jacobian approach are in good agreement with those computed by EC-OPE. A similar agreement is found for the vertical variation of the water vapor increments (not shown). Also, the number of iterations that is needed by the 1D-Var scheme to converge is about 25% smaller with the single mean Jacobian approach than with EC-OPE. This clearly indicates that the association of NeuroFlux and of the single mean Jacobian is reasonably consistent. Moreover, the use of a precomputed Jacobian is obviously faster than an explicit computation.

d. Summary

The neural network–based Jacobians contain features that are considered not to be realistic. During the learning phase of the neural networks, a nonlinear regression is performed to produce accurate fluxes and cooling rates. The inclusion of the Jacobians in the nonlinear regression would increase the number of constraints by two orders of magnitude. This can be achieved with more-complex neural networks, but the model would

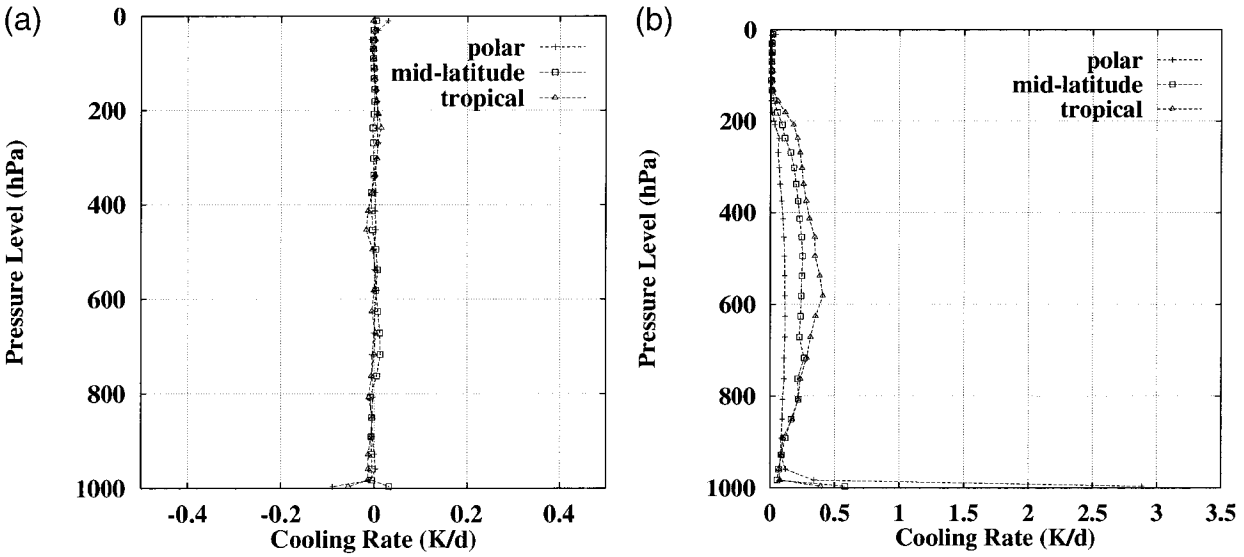

FIG. 4. (a) Mean and (b) std dev of the comparisons between tangent linear and nonlinear clear-sky cooling rates (K day^{-1}). The tangent linear approach uses a single mean Jacobian. The perturbations are taken from the difference between the ECMWF 6- and 12-h forecasts for 0000 UTC 1 Jul 1998. Results are shown in three latitude classes. On (b), the std dev of the error in the polar class reaches 3 K day^{-1} at the surface, whereas they are below 0.6 K day^{-1} in the other latitudes.

then be computationally less efficient. Now, the computational burden prevents EC-OPE to be introduced in the variational analysis, and faster solutions are studied. An approach for variational assimilation is proposed in which NeuroFlux only updates the fluxes in the minimization or recomputes the initial ones if the incremental 4D-Var is used. The gradient computation is performed with a single mean Jacobian. Results from both 1D-Var assimilation and tangent-linear approximation show that this approach is able to provide fast computations with good accuracy.

5. Comparison between RTTOV-5 and Synsatrad

a. General

RTTOV and Synsatrad already have been compared for brightness temperature and Jacobian computation in the Global Energy and Water Cycle Experiment Water Vapor Project, in which 23 models have been analyzed with respect to the 6.3-μm channel aboard *NOAA-14* (Soden et al. 2000). It was confirmed that Synsatrad is in better agreement with line-by-line models than is RTTOV. In particular, the behavior of RTTOV Jacobians for water vapor was shown to be significantly different from that of the other models. A comparison of some 19 models in the framework of the International ATOVS Working Group is enlarging the comparison to seven channels of HIRS (L. Garand 2000, personal communication). The current study completes these previous results. In addition to Eyre et al. (1993), who showed the positive impact of using RTTOV in the ECMWF analysis system through a 1D-Var retrieval, the current study compares its Jacobians with those from a more accurate scheme: Synsatrad. Compared with the previous Jacobian intercomparisons an interpretation of the Jacobians in terms of increments of geophysical quantities via the 1D-Var is provided here.

TABLE 1. First row of each section shows the mean (M) and std dev (σ) of the comparisons between tangent-linear (TL) and nonlinear (NL) clear-sky outgoing longwave radiation and clear-sky surface net flux perturbations. Middle row shows the mean and std dev of the NL clear-sky flux perturbations. Bottom row shows the mean and std dev of the NL total-sky flux perturbations. The perturbations are taken from the difference between the ECMWF 6- and 12-h forecasts for 0000 UTC 1 Jul 1998. Results (W m^{-2}) are shown in three lat classes.

	Polar		Midlatitude		Tropical	
	M	σ	M	σ	M	σ
			Outgoing longwave radiation			
TL − NL clear sky	−0.02	0.70	0.03	1.20	−0.14	1.46
NL clear sky	−0.13	1.49	−0.19	2.36	0.11	2.84
NL total sky	0.11	5.71	−0.19	11.78	0.74	17.27
			Surface net longwave flux			
TL − NL clear sky	−0.04	1.75	0.01	0.64	0.15	1.00
NL clear sky	0.16	2.94	0.04	4.52	−0.19	3.86
NL total sky	1.36	10.57	0.39	13.69	0.39	9.57

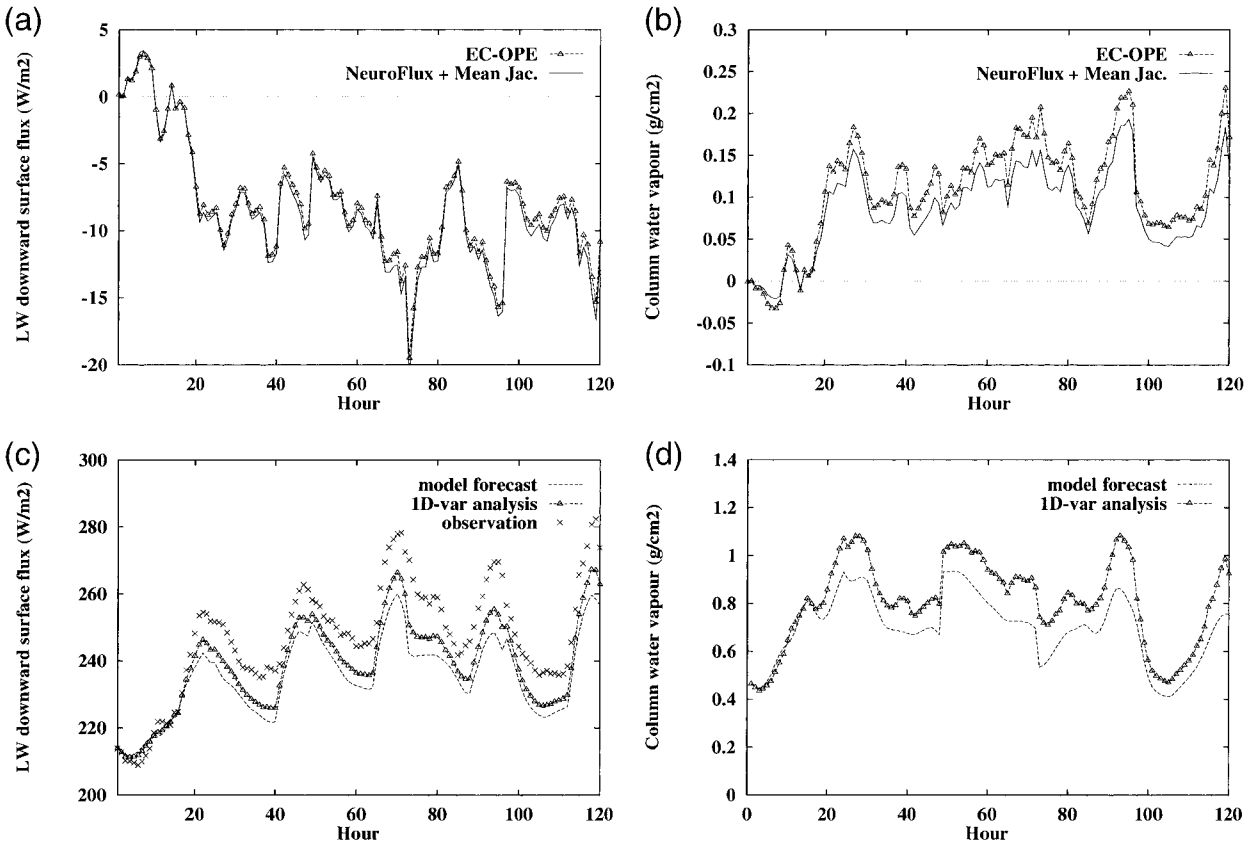

FIG. 5. (a) The difference between the downward longwave flux from a 1D-Var analysis using either EC-OPE or the single mean Jacobian approach and the flux measured at the ARM ''SGP'' site by a pyrgeometer. (b) The corresponding time series of total column water vapor increments. (c) Flux and (d) total column water vapor values for EC-OPE. In the single mean Jacobian approach, NeuroFlux is used to update the trajectory. The gradient computations are performed with a single mean Jacobian matrix.

b. Comparison of brightness temperatures

To compare RTTOV and Synsatrad, a representative set of atmospheric profiles is used (Chevallier 1999). It has been obtained by a random selection of 150 situations among a large set of 13 700 carefully sampled ECMWF global 6-h forecasts. Twenty-eight extreme profiles have been added. Unlike temperature and specific humidity, ozone comes from a climatological dataset that is dependent on season and latitude (Fortuin and Langematz 1994). To avoid any artifact due to orography, only profiles with a surface pressure higher than 950 hPa are used here: 103 cases. Forty-nine of them are taken from high- and midlatitude situations (i.e., latitudes higher than 30° in absolute value), and 54 are located in the tropical band. These profiles, defined on a 50-level vertical grid, are interpolated on the RTTOV fixed 43-level grid. Therefore, the radiation computations are performed at the same resolution for both RTTOV and Synsatrad.

Table 2 presents the comparison between RTTOV and Synsatrad for the computation of the brightness temperatures in channels HIRS-09, -10, -11, and -12 and Meteosat-WV. In the high- and midlatitude situations, mean differences are below 0.4 K with standard deviations up to 0.7 K. Differences are slightly higher for

TABLE 2. Statistics of the comparison of Synsatrad and RTTOV-5 for the computation of brightness temperatures (K).

	HIRS-09		HIRS-10		HIRS-11		HIRS-12		Meteosat WV	
	M	σ	M	σ	M	σ	M	σ	M	σ
High and midlatitudes										
RTTOV-5 − Synsatrad	−0.3	0.4	−0.1	0.2	0.4	0.4	0.3	0.7	0.0	0.7
Synsatrad	249.9	13.3	267.5	14.6	251.3	7.4	239.3	6.3	239.1	6.3
Tropical latitudes										
RTTOV-5 − Synsatrad	−0.6	0.1	−0.5	0.3	−0.1	0.5	−0.2	0.9	−0.9	1.0
Synsatrad	274.3	3.0	287.4	3.1	261.2	4.5	245.5	6.1	245.5	6.0

TABLE 3. Mean brightness temperature increment δT_b of the 1D-Var using either RTTOV-5 or Synsatrad.

	HIRS-09	HIRS-10	HIRS-11	HIRS-12	Meteosat WV
		High and midlatitudes			
Mean δT_b RTTOV-5	0.10	0.29	0.64	0.80	0.81
Mean δT_b Synsatrad	0.11	0.30	0.62	0.75	0.75
		Tropical latitudes			
Mean δT_b RTTOV-5	0.28	0.66	0.78	0.84	0.84
Mean δT_b Synsatrad	0.31	0.63	0.77	0.83	0.83

tropical latitudes, with biases and standard deviations up to 0.9 K. These numbers are comparable to the validation statistics of RTTOV-5, shown by Saunders et al. (1999), even if the sign of the biases may differ. Indeed, as explained in section 2b, Synsatrad solves the monochromatic radiative transfer equation and is therefore more accurate in principle than RTTOV-5 but is still not a line-by-line model. Differences in the reference line-by-line computations of the two schemes, like the water vapor continuum versions used [versions 2.1 and 2.2 of the Clough et al. (1989) parameterization], are not likely to affect the results to a significant extent. The higher bias occurs for Meteosat-WV in the Tropics: 0.9 K. It is associated with a standard deviation of 1 K. This bias is investigated further in section 5d.

c. Comparison of 1D-Var increments

The 1D-Var scheme described in section 3b allows for a further comparison between RTTOV-5 and Synsatrad. The global 103-profile set is used. The 1D-Var increments are computed on the 50-level grid so that the corresponding ECMWF error statistics can be applied. A vertical interpolation scheme is provided between the minimizer and the radiation models, which are both applied on the RTTOV fixed 43-level grid.

Simulated observations are constructed by adding 1 K to the 1D-Var first-guess brightness temperature with respect to each code. A 1-K standard deviation for the observation uncertainty is specified for each channel. Tests with a 0.5-K standard deviation show similar results, differing only in the amplitude of the signals. Resulting 1D-Var increments of temperature, water vapor, and ozone for each channel are examined. The conclusions for channels HIRS-11 and -12 and Meteosat-WV are very similar. Therefore, results for HIRS-11 and Meteosat-WV are not presented.

1) HIRS-09

As seen in Table 3, the 1D-Var brightness temperature increments are small for HIRS-09, in particular in the high- and midlatitude regions, for which the mean increment reaches 0.1 K only. Higher increments (0.3 K in the high- and midlatitude regions) can be obtained if surface temperature is introduced in the 1D-Var control variables. Note that the increments would reach 1 K if no background term was specified in the cost function [Eq. (5)]. Of course, they would be zero if the observation term was omitted. The corresponding Jacobians for ozone, shown in Fig. 6, peak at about 350 hPa, with higher values in the Tropics than in other latitudes,

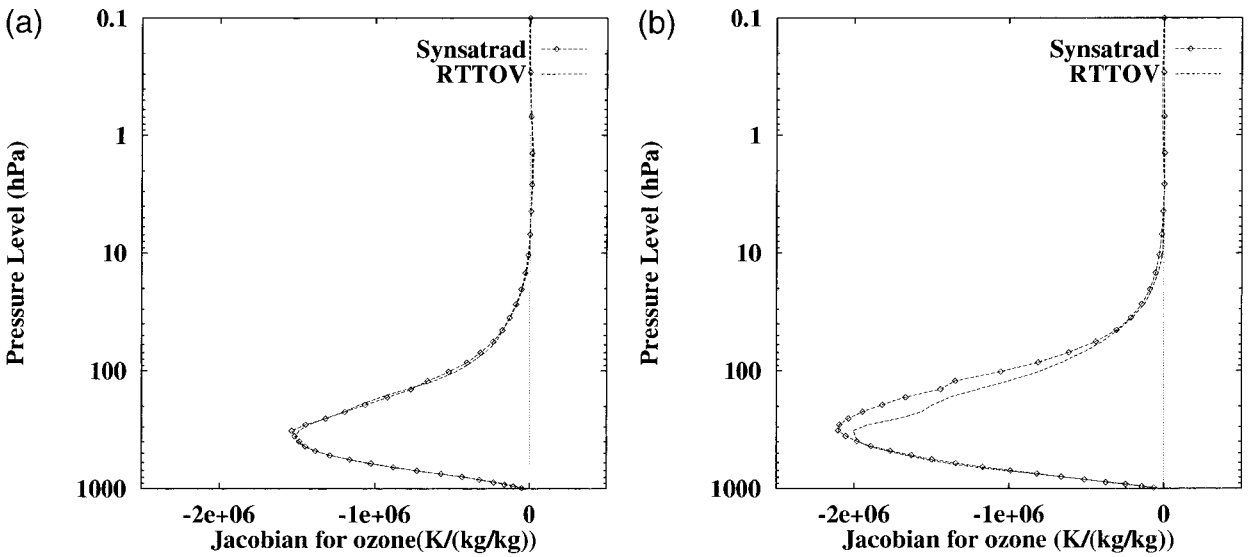

FIG. 6. For HIRS-09, mean Jacobian for ozone from Synsatrad and RTTOV for (a) high and midlatitudes and (b) tropical latitudes at the first iteration of 1D-Var.

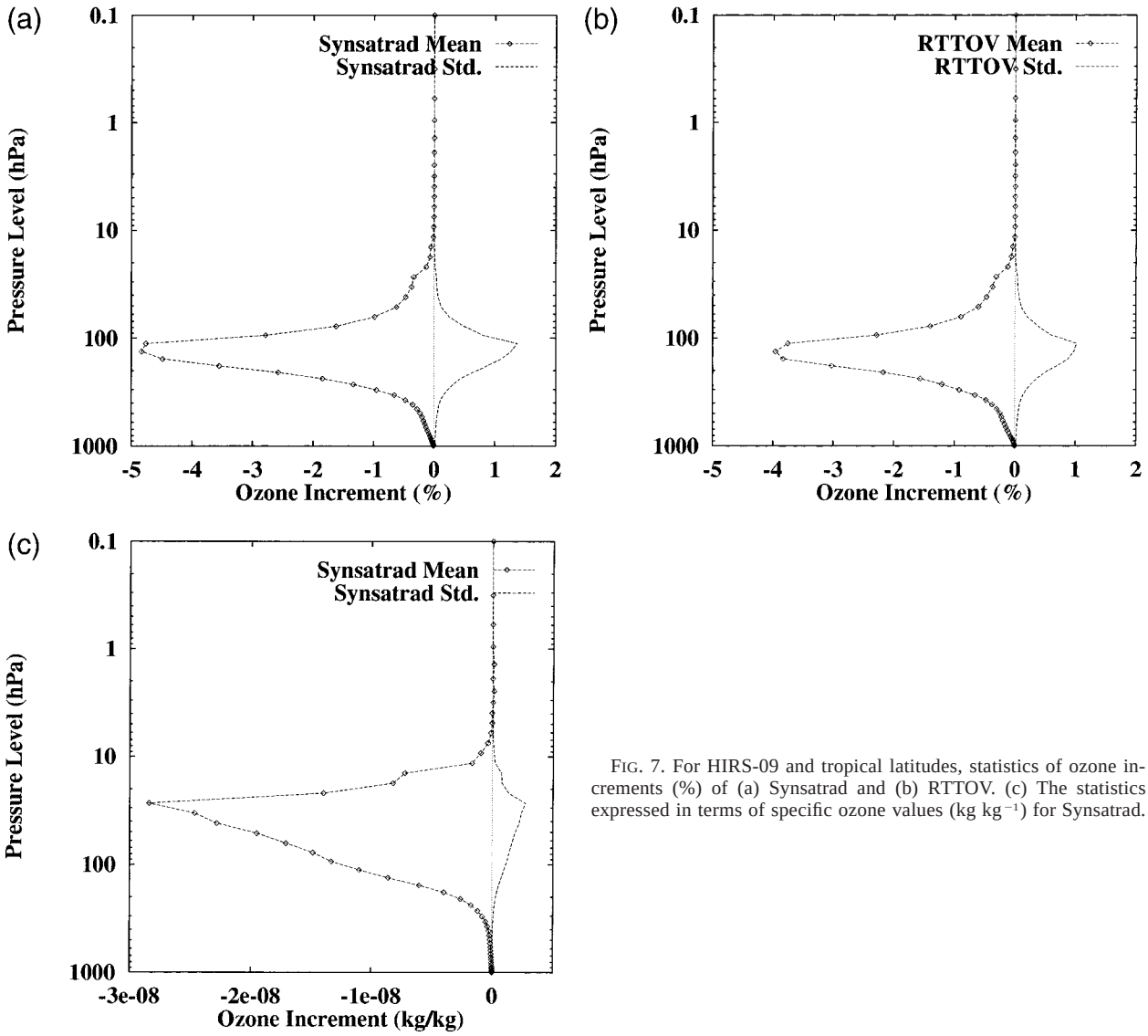

FIG. 7. For HIRS-09 and tropical latitudes, statistics of ozone increments (%) of (a) Synsatrad and (b) RTTOV. (c) The statistics expressed in terms of specific ozone values (kg kg^{-1}) for Synsatrad.

whereas the maximum values of the ozone profiles (kg kg^{-1}) occur at about 10 hPa. As a consequence, HIRS-09 is mostly sensitive to a region of the atmosphere in between, about 200 hPa, where only low increments of ozone (kg kg^{-1}) are allowed in the 1D-Var because of the background term, as shown in Fig. 1. As shown in Fig. 6, the RTTOV derivative values above 400 hPa are smaller than those of Synsatrad in the tropical regions. In the other regions, they are in good agreement.

The Jacobians for temperature, not shown, have their maximum higher in altitude, about 25 hPa, with a second local maximum at about 900 hPa. The corresponding temperature increments in the 1D-Var are very small in the tropical regions, less than 0.04 K, and are higher in the other latitudes, up to 0.2 K on average, with a good agreement between RTTOV and Synsatrad (not shown).

The ozone increments are shown in Fig. 7. Consistently with the previous comment, the specific ozone increments peak at about 30 hPa, whereas the relative change of ozone mostly occurs at 200 hPa. Because the gradient of the specified ozone error standard deviations (Fig. 1) is sharp at 200 hPa, the reduction of the Jacobian values above 400 hPa from Synsatrad to RTTOV makes the ozone increments smaller for RTTOV.

2) HIRS-10

The brightness temperature increments are larger for HIRS-10 than for HIRS-09: about 0.30 and 0.65 K, respectively, in the high- and midlatitude regions and in the tropical ones (Table 3). Jacobians have their maximum in the low troposphere for the temperature and near 450 hPa for the water vapor (see Fig. 8 for the high- and midlatitude regions). There is no ozone absorption in this channel. When compared with Synsa-

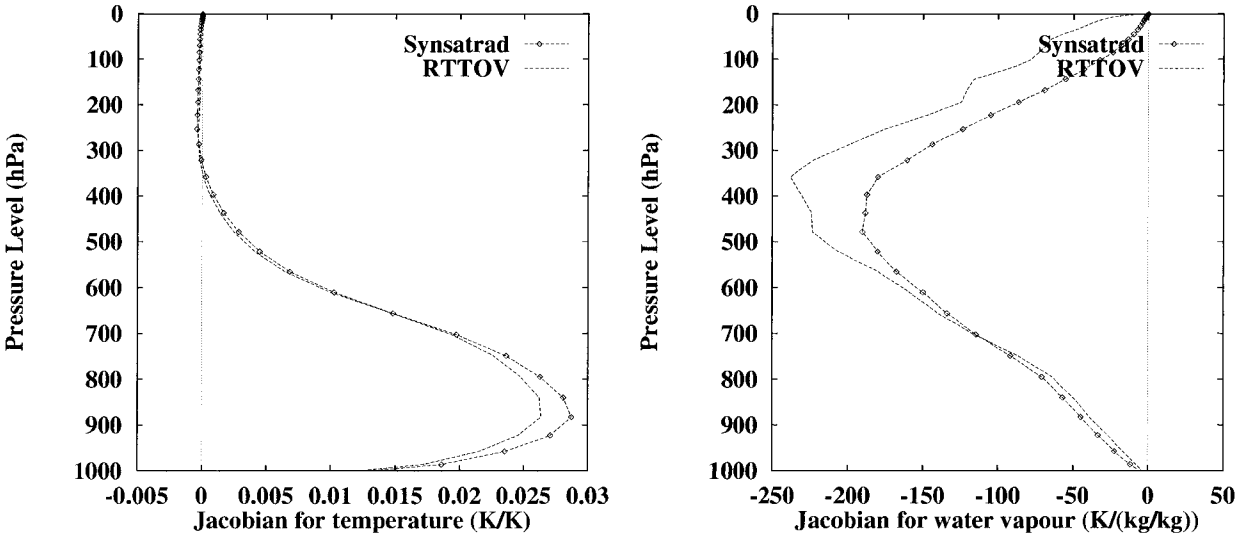

FIG. 8. For HIRS-10 and high and midlatitudes, mean Jacobians for (left) temperature and (right) water vapor from Synsatrad and RTTOV at the first iteration of 1D-Var.

trad, RTTOV-5 has smaller temperature Jacobians and larger, somewhat irregular, water vapor ones.

The 1D-Var temperature and water vapor increments are shown in Figs. 9 and 10 for the high- and midlatitude regions. The shape of the temperature increments reflects the specified background error covariance matrix, which includes negative correlations between temperature errors in the lower stratosphere and those in the troposphere (section 3c). Temperature and water vapor increments are similar for both models in value and shape. The Jacobian differences shown in Fig. 8 are not significant for variational data assimilation applications.

In the Tropics, the brightness temperature increments are mainly due to specific humidity. Water vapor increments are similar for both schemes (not shown).

3) HIRS-12

The brightness temperature increments for HIRS-12 are similar with RTTOV and Synsatrad: between 0.75 and 0.85 K (Table 3). Jacobians have their maximum at about 500 hPa for temperature and at about 250 hPa for water vapor (Fig. 11). If those for temperature are similar between the two models, the water vapor Jacobians have a clear and distinct behavior. The RTTOV values are more than 2 times as high as those of Synsatrad. Also, the maximum is higher in altitude with RTTOV. As expected, the increment difference appears more for water vapor than for temperature (Figs. 12 and 13). Indeed, mean relative changes of water vapor reach 40% with RTTOV at 200 hPa while not exceeding 20%

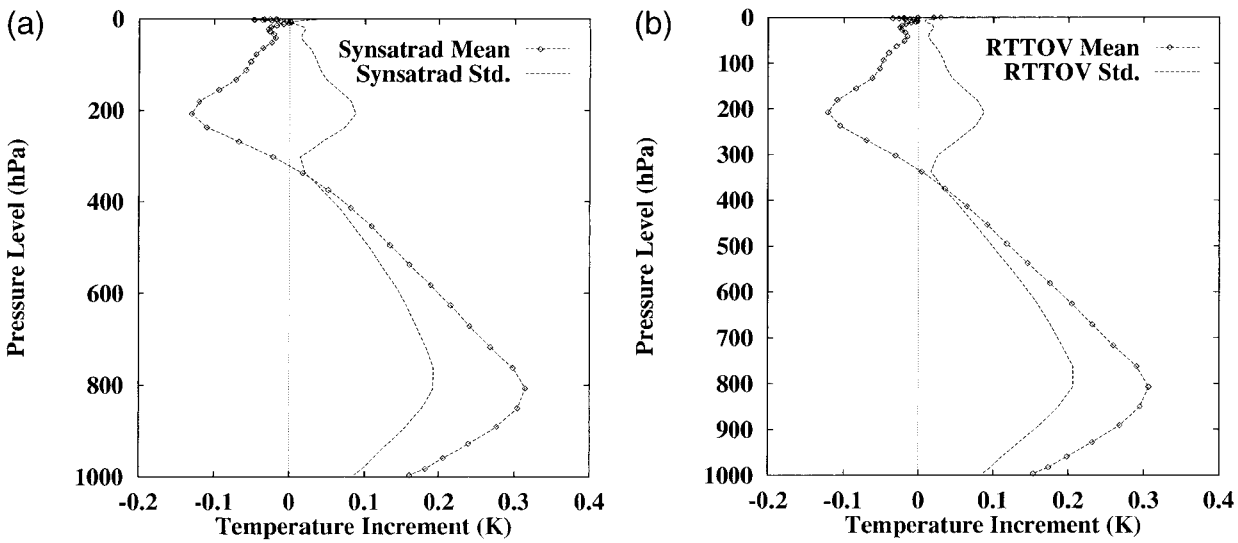

FIG. 9. For HIRS-10 and high and midlatitudes, statistics of the temperature increments from (a) Synsatrad and (b) RTTOV.

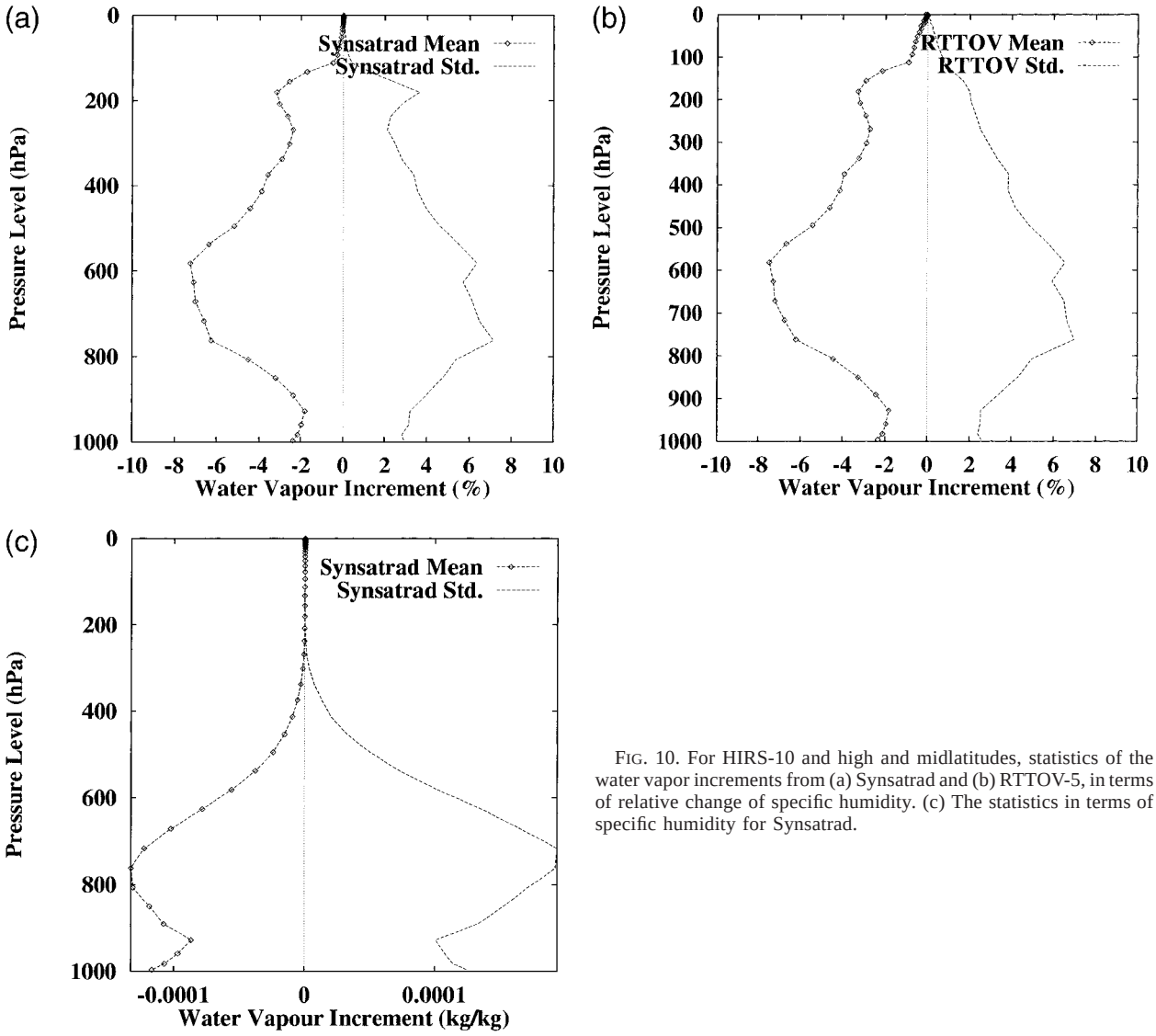

FIG. 10. For HIRS-10 and high and midlatitudes, statistics of the water vapor increments from (a) Synsatrad and (b) RTTOV-5, in terms of relative change of specific humidity. (c) The statistics in terms of specific humidity for Synsatrad.

with Synsatrad. Of course, these relative changes at 200 hPa correspond to small absolute amounts of water vapor (Fig. 13c).

d. Discussion

For the five channels studied (HIRS-09, -10, -11, and -12 and Meteosat-WV), differences in computed brightness temperatures between the RTTOV and Synsatrad have usually less than 0.5° bias and standard deviation. Jacobians for temperature appear to be in good agreement, and the width of HIRS-09 Jacobian for ozone in the tropical regions is higher with Synsatrad. The HIRS-11, HIRS-12, and Meteosat-WV Jacobians for water vapor are significantly different between the two codes in shape and in the vertical location of the maximum. Differences reduce for HIRS-10, which peaks lower in altitude.

These differences in Jacobians translate into differences in 1D-Var increments controlled by the specified background error statistics. As a consequence, the previous increment differences are mainly specific to ECMWF, from which system these statistics were taken. In this study, only water vapor increments for HIRS-11, HIRS-12, and Meteosat-WV significantly differ between the two models.

Because of the use of a more physical computation method, Jacobians of Synsatrad are expected to be closer to the truth than those of RTTOV. Soden et al. (2000) also show a deficiency of HIRS-12 RTTOV Jacobians for water vapor. As described in section 2b, RTTOV is based on two approximations: the invariance of the Planck function on the channel width and the computation of optical depths through a linear regression.

The first approximation is explored with Synsatrad as follows. Single-band convolved transmissions are

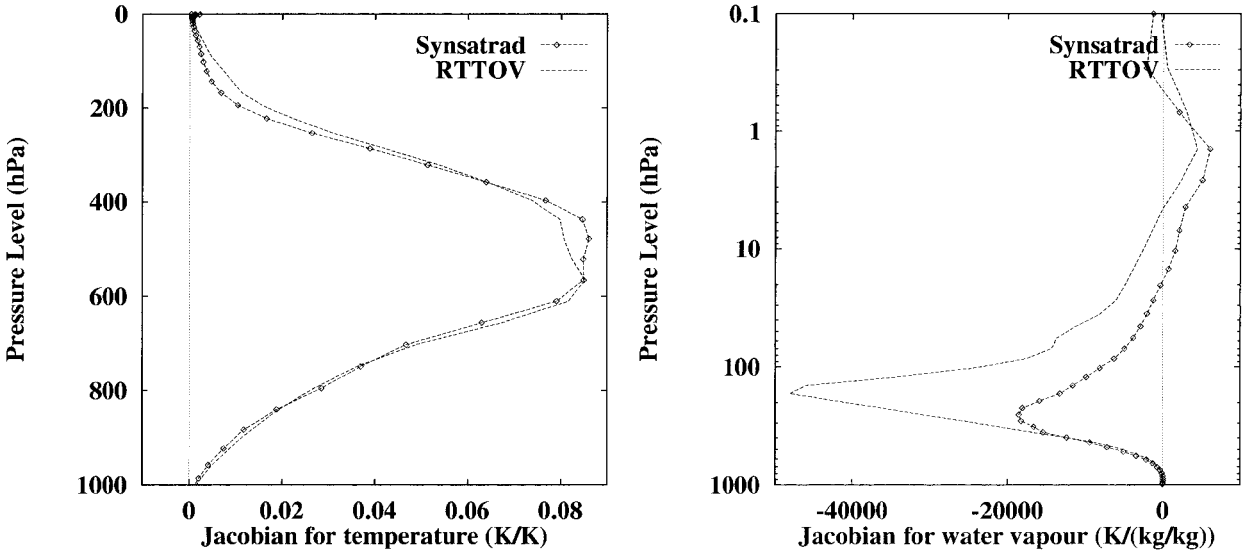

FIG. 11. For HIRS-12 and high and midlatitudes, mean Jacobians for (left) temperature and (right) water vapor from Synsatrad and RTTOV at the first iteration of 1D-Var.

computed with the narrowband model for the five channels considered here. They are used to calculate the radiance L_i in a channel i in a way that is consistent with RTTOV-5:

$$L_i = B_i(T_{N+1})\tau_i(N+1) + \sum_{k=1}^{N} B_i(T_k)[\tau_i(k) - \tau_i(k+1)], \quad (9)$$

where N is the number of vertical layers, $B_i(T)$ is the mean Planck function in channel i for temperature T, $\tau_i(k)$ is the convolved transmittance in channel i from the top of the atmosphere (level 1) to level k, and T_k is mean temperature in layer k.

Statistics of the difference between the approximate brightness temperatures and the full Synsatrad computation on the 103-profile dataset are shown in Table 4. Biases and standard deviations are below 0.1 K in absolute value for all channels except for Meteosat-WV, for which a bias of 0.5 K is found. This bias carries the same sign as the one between RTTOV and Synsatrad but is not latitude-dependent as the latter is (see Table 2). Indeed, different sources of error add or compensate between RTTOV and Synsatrad. Table 4 suggests that the invariant-Planck-function approximation is important to explain the differences observed for Meteosat-WV. This is not surprising, given the Meteosat-WV spectral width, which ranges from 1350 to 1850 cm^{-1},

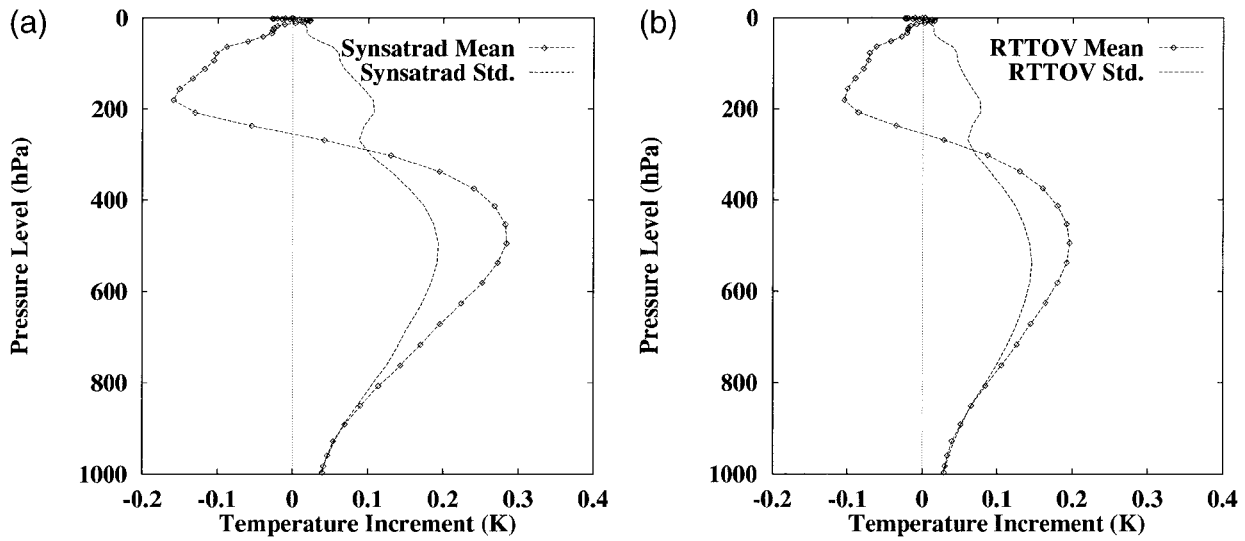

FIG. 12. For HIRS-12 and high and midlatitudes, statistics of the temperature increments from (a) Synsatrad and (b) RTTOV.

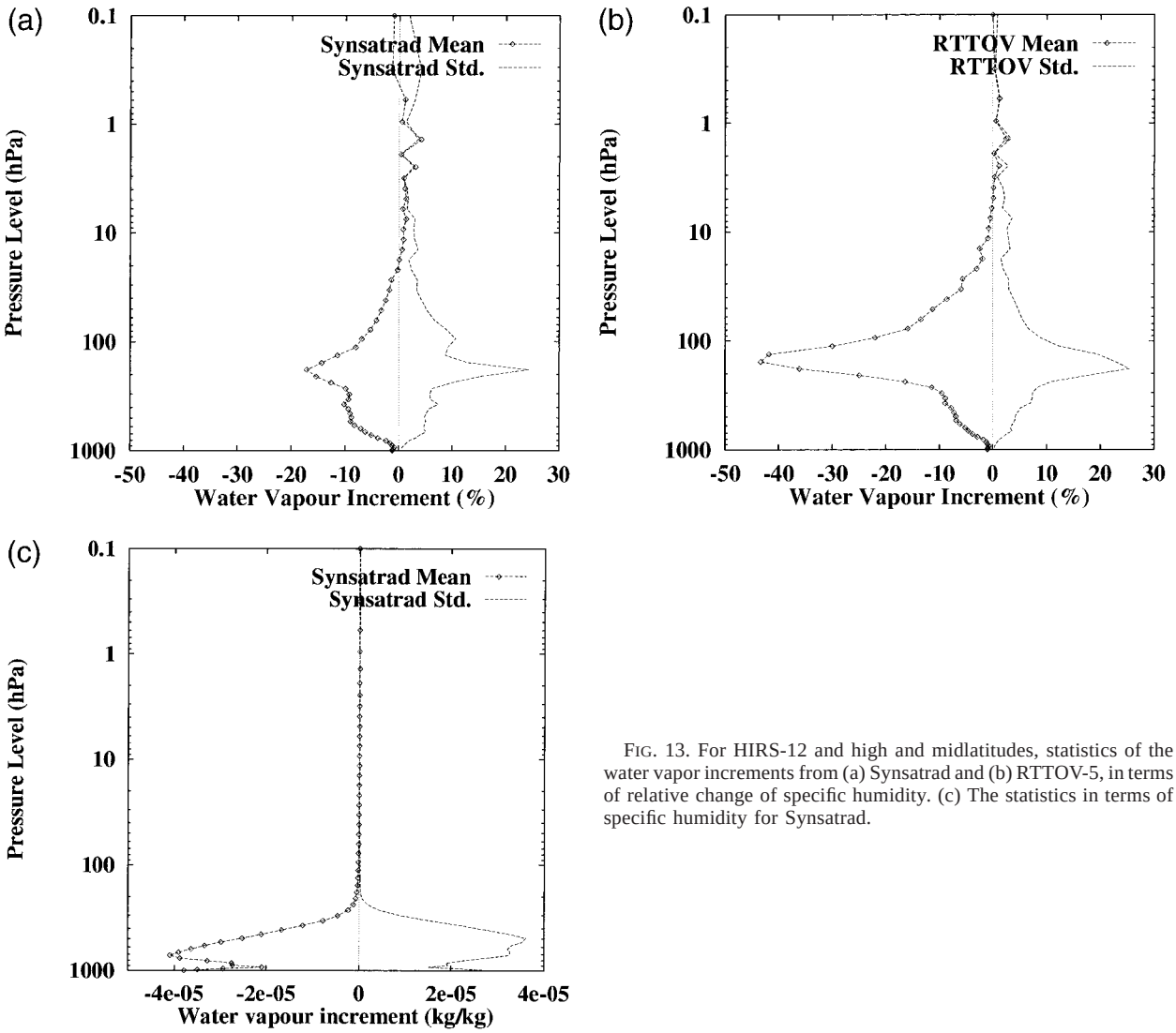

FIG. 13. For HIRS-12 and high and midlatitudes, statistics of the water vapor increments from (a) Synsatrad and (b) RTTOV-5, in terms of relative change of specific humidity. (c) The statistics in terms of specific humidity for Synsatrad.

as compared with HIRS-12, which ranges from 1420 to 1560 cm^{-1} only. The low associated standard deviation (0.1 K) suggests that a simple bias correction is able to remove that particular problem. For the Jacobians, only a small impact is found on Meteosat-WV as well as on HIRS-12 (not shown).

TABLE 4. Test of the impact of the spectral integration approximation used in RTTOV. Difference between the computation of brightness temperature with Synsatrad in the narrowband mode and that with Synsatrad using the approximation [approximation minus narrowband (K)].

	High and midlatitudes		Tropical latitudes	
	M	σ	M	σ
HIRS-09	−0.1	0.0	−0.1	0.0
HIRS-10	0.0	0.0	0.0	0.0
HIRS-11	0.1	0.0	0.1	0.0
HIRS-12	−0.2	0.1	−0.1	0.1
Meteosat WV	−0.5	0.1	−0.5	0.1

Therefore, the second approximation on which RTTOV relies, namely the use of a linear regression to derive the optical depths, is likely to be responsible for the low accuracy of RTTOV 6.3 and 7.3 μm water vapor Jacobians. Improvements of RTTOV are expected from a better quality of the regression dataset (e.g., Chevallier 1999) and from more adequate predictors (e.g., Matricardi and Saunders 1999). The interpolation of the water vapor profiles of the current regression dataset between 100 and 300 hPa (as explained by Saunders et al. 1999) may be the main reason for the bad Jacobians (R. Saunders 2000, personal communication; see also Fig. 11b).

6. Conclusions

Variational methods are increasingly used for data assimilation in operational weather centers. They provide statistically optimal analyses of the atmosphere when error statistics and Jacobians are correctly spec-

ified. The evaluation of Jacobians for variational data assimilation has to be related to the complete framework, including the specified error statistics. As an example, the differences between RTTOV and Synsatrad Jacobians were shown to be strongly influenced by these statistics when they are converted into 1D-Var increments.

Neural network–based Jacobians for broadband infrared radiation were shown to be deficient for water vapor. However, the random structure of the derivative error allows the use of NeuroFlux with a single mean Jacobian in the variational context. Errors produced by this approach are small. Clouds are the major modulator of fluxes and cooling rates and are accounted for in the framework of the multilayer graybody approach. Therefore, accurate and fast longwave broadband radiation computations can be introduced in 4D-Var with the single mean Jacobian approach to compute increments and derivatives and NeuroFlux to recompute the trajectory around which the linearization is performed.

For satellite brightness temperature modeling, RTTOV Jacobians were also shown to be deficient for water vapor for the 6.3- and 7.3-μm channels, with a significant impact on the 1D-Var retrievals. The mean shape of the increments is similar to those of Synsatrad, but the signal amplitude differs. Because the RTTOV increment shape is good, the inclusion of RTTOV in variational data analysis for the assimilation of such channels positively affects the quality of the operational analyses and forecasts, particularly in the Southern Hemisphere and the Tropics (McNally and Vespérini 1996). Smaller weaknesses for temperature and ozone and for water vapor in the 12.5-μm channel (HIRS-10) do not significantly affect the increments. Further improvements to RTTOV are expected from ongoing work in the framework of the Numerical Weather Prediction Satellite Application Facility funded by EUMETSAT, where both the regression dataset and the choice of the predictors are being revised.

Acknowledgments. This work was done at the Satellite Application Facility on Numerical Weather Prediction, which is cosponsored by EUMETSAT. The authors thank F. Aires and A. Chédin for fruitful discussions about the neural network–based Jacobians. For the comparison between RTTOV and Synsatrad, special thanks go to R. Saunders and S. Tjemkes. The kind help of G. Kelly, R. Munro, and E. Holm at various stages of the work was appreciated. F. Bouttier provided the statistics of forecast errors from the ECMWF operational data assimilation system. INRIA provided the M1QN3 minimization code. M. Janisková, T. McNally, J.-J. Morcrette, and R. Saunders helped to improve the initial manuscript.

REFERENCES

Aires, F., M. Schmitt, A. Chédin, and N. A. Scott, 1999: The ''weight smoothing'' regularization of MLP for Jacobian stabilization. *IEEE Trans. Neural Networks,* **10** (6), 1502–1510.

Chéruy, F., F. Chevallier, J.-J. Morcrette, N. A. Scott, and A. Chédin, 1996: Une méthode utilisant les techniques neuronales pour le calcul rapide de la distribution verticale du bilan radiatif thermique terrestre (A fast method using neural networks for computing the vertical distribution of the thermal component of the Earth radiative budget). *C. R. Acad. Sci. Paris,* **322** (IIb), 665–672.

Chevallier, F., 1998: La modélisation du transfert radiatif à des fins climatiques: Une nouvelle approche fondée sur les réseaux de neurones artificiels (The modeling of radiative transfer for climatic purposes: A new approach based on articficial neural networks). Ph.D. thesis, University Paris VII, 230 pp. [Available from LMD, Ecole Polytechnique, 91128 Palaiseau cedex, France.]

——, 1999: TIGR-like sampled databases of atmospheric profiles from the ECMWF 50-level forecast model. ECMWF/Eumetsat NWP SAF Res. Rep. 1, 18 pp.

——, and J.-J. Morcrette, 2000: Comparison of model fluxes with surface and top-of-the-atmosphere observations. *Mon. Wea. Rev.,* **128,** 3839–3852.

——, F. Chéruy, N. A. Scott, and A. Chédin, 1998: A neural network approach for a fast and accurate computation of longwave radiative budget. *J. Appl. Meteor.,* **37,** 1385–1397.

——, A. Chédin, F. Chéruy, and J.-J. Morcrette, 2000a: TIGR-like atmospheric situation databases for accurate radiative flux computation. *Quart. J. Roy. Meteor. Soc.,* **126,** 777–785.

——, J.-J. Morcrette, F. Chéruy, and N. A. Scott, 2000b: Use of a neural network-based longwave radiative transfer scheme in the ECMWF atmospheric model. *Quart. J. Roy. Meteor. Soc.,* **126,** 761–776.

Clough, S. A., F. X. Kneizys, and R. Davies, 1989: Line shape and the water vapor continuum. *Atmos. Res.,* **23,** 229–241.

Courtier, P., J.-N. Thépaut, and A. Hollingsworth, 1994: A strategy, for operational implementation of 4D-Var, using an incremental approach. *Quart. J. Roy. Meteor. Soc.,* **120,** 1367–1388.

——, and Coauthors, 1998: The ECMWF implementation of three dimensional variational assimilation (3D-Var). Part I: Formulation. *Quart. J. Roy. Meteor. Soc.,* **124,** 1783–1808.

Derber, J., and F. Bouttier, 1999: A reformulation of the background error covariance in the ECMWF global data assimilation system. *Tellus,* **51A,** 195–221.

Ebert, E. E., and J. A. Curry, 1992: A parameterization of ice optical properties for climate models. *J. Geophys. Res.,* **97,** 3831–3836.

Edwards, D. P., 1992: GENLN2. A general line-by-line atmospheric transmittance and radiance model. NCAR Tech. Note NCAR/TN-367+STR, National Center for Atmospheric Research, Boulder, CO, 157 pp.

Eyre, J. R., 1991: A fast radiative transfer model for satellite sounding systems. ECMWF Tech. Memo. 176, 28 pp.

——, G. A. Kelly, A. P. McNally, E. Andersson, and A. Persson, 1993: Assimilation of TOVS radiance information through one-dimensional variational analysis. *Quart. J. Roy. Meteor. Soc.,* **119,** 1427–1463.

Fillion, L., and J.-F. Mahfouf, 2000: Coupling of moist-convective and stratiform precipitation processes for variational data assimilation. *Mon. Wea. Rev.,* **128,** 109–124.

Fortuin, J. P. F., and U. Langematz, 1994: An update on the global ozone climatology and on concurrent ozone and temperature trends. *Proc. of the Int. Society for Optical Engineering on Atmospheric Sensing and Modeling,* Vol. 2311, Rome, Italy, SPIE, 207–216.

Geleyn, J.-F., and A. Hollingsworth, 1979: An economical analytical method for the computation of the interaction between scattering and line absorption in radiation. *Beitr. Phys. Atmos.,* **52,** 1–16.

Gilbert, J. C., and C. Lemaréchal, 1989: Some numerical experiments with variable-storage quasi-Newton algorithms. *Math. Programming,* **45,** 407–435.

Gregory, D., J.-J. Morcrette, C. Jakob, and A. Beljaars, 1998: Introduction of revised radiation, convection, cloud and vertical dif-

fusion schemes into Cy18r3 of the ECMWF integrated forecasting system. ECMWF Tech. Memo. 254, 39 pp.

Heimo, A., A. Vernez, and P. Wasserfallen, 1993: Baseline Surface Radiation Network (BSRN). Concept and implementation of a BSRN station. WMO/TD No. 579, WCRP/WMO, Geneva, 17 pp.

Hollingsworth, A., 1987: Objective analysis for numerical weather prediction. *Short and Medium Range Numerical Weather Prediction, Special Volume Journal of the Meteorological Society of Japan,* T. Matsumo, Ed., Meteorological Society of Japan, 11–60.

Janisková, M., J.-N. Thépaut, and J.-F. Geleyn, 1999: Simplified and regular physical parameterizations for incremental four-dimensional variational assimilation. *Mon. Wea. Rev.,* **127,** 26–45.

Le Dimet, F.-X., and O. Talagrand, 1986: Variational algorithms for analysis and assimilation of meterological observations. *Tellus,* **38A,** 97–110.

Lewis, J. M., and J. C. Derber, 1985: The use of adjoint equations to solve a variational adjustment problem with advective constraints. *Tellus,* **37A,** 309–322.

Mahfouf, 1999: Influence of physical processes on the tangent-linear approximation. *Tellus,* **51A,** 147–166.

Marécal, V., and J.-F. Mahfouf, 1999: Variational retrieval of temperature and humidity profiles from TRMM precipitation data. ECMWF Tech. Memo. 293, 28 pp.

Matricardi, M., and R. Saunders, 1999: Fast radiative transfer model for simulation of infrared atmospheric sounding interferometer radiances. *Appl. Opt.,* **38,** 5679–5691.

McClatchey, R. A., R. W. Fenn, J. E. A. Selby, F. E. Volz, and J. S. Garing, 1971: Optical properties of the atmosphere. AFCRL Tech. Note AFCRL-TR-73-0096, Air Force Cambridge Res. Lab., Bedford, MA, 94 pp.

McMillin, L. M., H. E. Fleming, and M. L. Hill, 1979: Atmospheric transmittance of an absorbing gas. 3: A computationally fast and accurate transmittance model for absorbing gases with variable mixing ratios. *Appl. Opt.,* **18,** 1600–1606.

McNally, A. P., 2000: Estimates of short-range forecast-temperature error correlations and the implications for radiance-data assimilation. *Quart. J. Roy. Meteor. Soc.,* **126,** 361–373.

——, and M. Vespérini, 1996: Variational analysis of humidity information from TOVS radiances. *Quart. J. Roy. Meteor. Soc.,* **122,** 1521–1544.

Morcrette, J.-J., 1991: Radiation and cloud radiative properties in the European Centre for Medium-Range Weather Forecasts forecasting system. *J. Geophys. Res.,* **96,** 9121–9132.

——, 2000: On the effects of the temporal and spatial sampling of radiation fields on the ECMWF forecasts and analyses. *Mon. Wea. Rev.,* **128,** 876–887.

Parrish, D. F., and J. C. Derber, 1992: The National Meteorological Center's spectral statistical interpolation analysis system. *Mon. Wea. Rev.,* **120,** 1747–1763.

Rabier, F., A. McNally, E. Andersson, P. Courtier, P. Unden, J. Eyre, A. Hollingsworth, and F. Bouttier, 1998: The ECMWF implementation of three dimensional variational assimilation (3D-Var). Part II: Structure functions. *Quart. J. Roy. Meteor. Soc.,* **124,** 1809–1829.

Rumelhart, D. E., G. E. Hinton, and R. J. Williams, 1986: Learning internal representations by error propagation. *Parallel Distributed Processing: Explorations in the Macrostructure of Cognition 1,* D. E. Rumelhart and J. L. McClelland, Eds., MIT Press, 318–362.

Sasaki, Y., 1958: An objective analysis based on the variational method. *J. Meteor. Soc. Japan,* **36,** 738–742.

Saunders, R., M. Matricardi, and P. Brunel, 1999: An improved fast radiative transfer model for assimilation of satellite radiance observations. *Quart. J. Roy. Meteor. Soc.,* **125,** 1407–1425.

Sneden, C., H. Johnson, and B. Krupp, 1975: A statistical method for treating molecular line opacities. *Astrophys. J.,* **204,** 281–289.

Soden, B., and Coauthors, 2000: An intercomparison of radiation codes for retrieving upper tropospheric humidity in the 6.3-μm band: A report from the first GVaP workshop. *Bull. Amer. Meteor. Soc.,* **81,** 797–808.

Stokes, G. M., and S. E. Schwartz, 1994: The Atmospheric Radiation Measurement (ARM) Program: Programmatic background and design of the Cloud and Radiation Testbed. *Bull. Amer. Meteor. Soc.,* **75,** 1201–1221.

Tjemkes, S. A., and J. Schmetz, 1997: Synthetic satellite radiances using the radiance sampling method. *J. Geophys. Res.,* **102,** 1807–1818.

Washington, W. M., and D. L. Williamson, 1977: A description of the NCAR GCMs. *General Circulation Models of the Atmosphere. Methods in Computational Physics,* J. Chang, Ed., Vol. 17, Academic Press, 111–172.